Technobius Physics, 2026, 4(1), 0045, DOI: https://doi.org/10.54355/tbusphys/4.1.2026.0045

Technobius Physics

https://technobiusphysics.kz/

e-ISSN 3007-0147

Article

Standardized extraction of optical band gap and urbach energy in zno and al-doped zno thin films from uv–vis spectra: an in-silico workflow

Do-Yoon Lee*, Gye-Tai Park

College of Science, Department of Physics, Younsei University, Seoul, South Korea
*Correspondence: doyooonlee@gmail.com

Abstract. This study develops and validates a reproducible computational workflow for extracting the optical band gap and Urbach tail parameters of ZnO and Al-doped ZnO thin films from UV–Vis spectra. Synthetic transmission datasets were generated for ZnO and ZnO:Al (0–3 at.% Al) using a physically consistent thin-film optics model with realistic spectral broadening and noise, followed by standardized post-processing to reconstruct absorption behavior and perform band-edge analysis. The optical band gap values derived from the band-edge region remained tightly clustered across all compositions, with group means near 3.31–3.33 eV and small between-replicate dispersion (standard deviation ≤ 0.005 eV), indicating robust gap extraction under a fixed regression protocol. In contrast, the Urbach energy exhibited substantially higher variability, with group means spanning approximately 37–112 meV and larger scatter, highlighting the greater sensitivity of sub-gap analysis to low-signal regions and fitting-window selection. Overall, the results demonstrate that band-gap estimation is comparatively stable when procedures are standardized, whereas Urbach-tail quantification requires stricter control of noise floor and objective windowing. The proposed workflow provides a transparent baseline for consistent reporting and can be directly transferred to experimental ZnO/AZO datasets; the main limitation is that the present results are derived from synthetic spectra, motivating future validation on measured thin-film optical data.

Keywords: ZnO thin films, Al-doped ZnO (AZO), optical band gap, urbach energy, UV–Vis spectroscopy.

1. Introduction

Transparent wide-band-gap oxide semiconductors are central to thin-film optoelectronics because they can transmit most visible light while still providing strong absorption and electronic functionality in the near-UV. ZnO is a prototypical wide-band-gap oxide used in coatings, photodetectors, sensors, and transparent conducting architectures due to its robust optical edge and compatibility with multiple deposition routes [1], [2], [3]. A widely used approach to tailor ZnO is donor doping with aluminum (ZnO:Al, often termed AZO), which can modify carrier density, defect chemistry, and microstructure, thereby changing the absorption edge position and its sharpness—two aspects that directly affect transparency–performance trade-offs in functional films [4], [5], [6].

In routine practice, the optical edge of ZnO-based films is quantified by extracting (i) an optical band gap from the near-edge absorption rise and (ii) an Urbach energy from the exponential absorption tail below the edge. The band gap is commonly estimated using Tauc-type regression, whereas the Urbach energy is obtained from a linear fit of the logarithm of absorption versus photon energy in the sub-gap region. Although these two parameters are conceptually simple, their reported values often vary substantially across studies because thin-film UV–Vis spectra are rarely ideal: interference fringes, baseline drift, scattering, and low-signal artifacts can distort the apparent edge, while the selection of fitting windows and preprocessing steps can dominate the regression outcome [7]. As a result, disagreements in the literature may reflect analysis choices as much as material physics.

Recent original research on ZnO and AZO highlights this methodological sensitivity. Electrospray-deposited AZO films have been analyzed via UV–Vis transmission to optimize optical–functional performance, yet the extracted edge parameters depend on how the edge region is selected and treated across samples [8]. Sol–gel spin-coated AZO waveguide films similarly demonstrate composition-dependent optical behavior; however, the optical edge analysis remains protocol-driven, particularly under variable interference/background conditions in thin coatings [9]. Studies that explicitly calculate dispersion/absorption-edge parameters for AZO report meaningful trends, but commonly provide limited replication and do not always separate uncertainty due to sub-gap noise from true disorder changes [10]. Broader comparisons across doped ZnO thin films (including Al-doping) show that "band-gap shift" is not universally monotonic with dopant content and may couple strongly to microstructure and defect populations rather than to nominal composition alone [11]. Work on Al-doped ZnO further demonstrates that optical changes are often interpreted through competing mechanisms (carrier filling and edge shift versus disorder-driven broadening), which become difficult to disentangle when extraction protocols differ [12]. Focused absorption-edge studies on nanostructured AZO thin films confirm that both edge shift and edge broadening can occur simultaneously and that Urbach-tail metrics may correlate with microstructural evolution, again underscoring the need for consistent, reproducible fitting strategies [10]. Parallel investigations of defected ZnO films show that Urbach-tail parameters can track disorder/defect signatures observed in complementary probes, but also that the sub-gap region is the most sensitive part of the spectrum to noise-floor and baseline choices [13]. Importantly, even when studies target other optical figures of merit (e.g., nonlinear optical response or sensing performance), they still rely on band-edge extraction from UV–Vis measurements, reinforcing that robust and comparable band-edge metrics are a cross-cutting requirement in ZnO thin-film research [12], [14]. At the application scale, large-area growth of AZO transparent conducting films continues to require reliable optical-edge metrics for screening and reproducibility, amplifying the consequences of inconsistent extraction procedures [9]. Likewise, architectural tuning approaches (e.g., multilayer ZnO stacks) routinely report optical edge changes, making cross-study comparability essential for meaningful design rules [15].

Research gap. Despite extensive experimental work on ZnO/AZO, the field still lacks a widely transferable, end-to-end extraction workflow that (i) uses objective and repeatable windowing rules for band gap and Urbach fits, (ii) explicitly separates near-edge gap estimation from sub-gap tail behavior, and (iii) quantifies variability across replicates so that analysis uncertainty is not conflated with material trends [4], [7], [9].

Hypothesis. If band-edge extraction is performed using a standardized protocol with replicate-based statistics, then the band-gap estimate will show comparatively low dispersion within a dataset, whereas Urbach energies will remain more sensitive to the sub-gap spectral region and fitting-window selection, reflecting their stronger dependence on low-absorption data quality [1], [5], [11].

Goal and novelty. The goal of this study is to develop and demonstrate a fully reproducible workflow for ZnO and ZnO:Al thin films that links UV–Vis spectra to absorption reconstruction and standardized extraction of optical band gap and Urbach energy, including replicate statistics. The novelty lies in providing a transparent, protocol-controlled baseline (spectra → processing → parameters → variability) designed specifically to improve the comparability and interpretability of ZnO/AZO band-edge reporting.

2. Methods

2.1. Study design and datasets

This work was conducted as an in-silico thin-film optics study designed to validate a reproducible workflow for extracting the optical band gap and Urbach energy from UV–Vis spectra of ZnO and Al-doped ZnO (ZnO:Al, AZO) thin films. The computational design explicitly targets the main source of disagreement in the literature, namely protocol-dependent fitting-window selection and sub-gap noise sensitivity, by enforcing fixed decision rules and replicate-based

statistics. Two material systems were considered: undoped ZnO and ZnO:Al. For ZnO:Al, four nominal Al contents were simulated: 0, 1, 2, and 3 at.% (used as dataset labels). For each composition group, n = 10 independent virtual films were generated to enable within-group statistics and to quantify protocol stability. Table 1 lists all simulation inputs and perturbations required to reproduce the dataset generation and the subsequent extraction pipeline.

Table 1 – Key in-silico simulation inputs and perturbation settings used to generate UV–Vis spectra for ZnO and ZnO:Al datasets

Category	Setting	Notes
Spectral range	300–900 nm; step 1 nm	Normal incidence
Compositions	ZnO; ZnO:Al (0–3 at.% Al labels)	Four groups
Replicates	n = 10 per group	Used for mean ± SD
Thickness d	ZnO: 250–450 nm; ZnO:Al: 200–400 nm	5% coefficient of variation
Instrument broadening	Gaussian FWHM = 2 nm	Applied to spectra
Noise model	Gaussian noise: σ(T)=0.2%, σ(R)=0.3%	Additive
Baseline drift	<0.3% low-order polynomial	Uniform rule
Band-edge parameterization	Tauc onset + Urbach tail	Continuity enforced
Statistics	Bootstrap residual resampling (1000)	95% CI for Eg and EU

2.2. Optical model of a thin absorbing film on a transparent substrate

Synthetic normal-incidence transmission spectra T(λ) and reflectance spectra R(λ) were generated for a single absorbing thin film on a transparent substrate using the transfer-matrix (characteristic-matrix) formalism for stratified media. The film was treated as optically coherent, while the substrate was treated as optically thick (incoherent), which is a standard approximation for spectrophotometric measurements on millimeter-scale transparent substrates. The film optical response was described by the complex refractive index

$$\tilde{n}(\lambda) = n(\lambda) + ik(\lambda) \quad (1)$$

In the weak-absorption (transparent) region, the dispersion of n(λ) was represented by a Cauchy model

$$n(\lambda) = A + \frac{B}{\lambda^2} + \frac{C}{\lambda^4} \quad (2)$$

where λ is in nanometers and A, B, C are fixed coefficients kept identical within each composition group to avoid introducing additional degrees of freedom unrelated to the band-edge analysis. The substrate refractive index was treated as constant over 300–900 nm for the purpose of spectrum generation.

2.3. Band-edge parameterization: Tauc onset and Urbach tail

The absorption coefficient α(hν) was parameterized to contain both a near-edge Tauc-type onset and a sub-gap Urbach exponential tail, with continuity enforced between the two regimes to avoid artificial discontinuities in α(hν). For the Tauc regime, the direct-allowed transition convention was used:

$$(\alpha h\nu)^m = A_T(h\nu - E_g), m = \frac{1}{2} \quad (3)$$

where $h\nu$ is photon energy, A_T is a proportionality constant, and E_g is the optical band gap. For the Urbach regime, the exponential tail was modeled as:

$$\alpha(h\nu) = \alpha_0 exp\left(\frac{h\nu - E_1}{E_U}\right) \quad (4)$$

where α0 and E1 are fitting parameters and E_U is the Urbach energy. The extinction coefficient was computed from α via:

$$k(\lambda) = \frac{\alpha(\lambda)\lambda}{4\pi} \quad (5)$$

This construction ensures that the synthetic spectra contain an explicit, physically interpretable tail region and a near-edge onset that can be recovered by the same regression-based procedures commonly applied to experimental UV–Vis data.

2.4. Thickness and variability settings

Film thickness was assigned per virtual sample within realistic ranges and perturbed to emulate fabrication variability: ZnO: 250–450 nm; ZnO:Al: 200–400 nm. Thickness values were sampled from a normal distribution with a 5% coefficient of variation within each group. To emulate microstructural variability beyond thickness spread, Eg and EU were also perturbed within each group using normal distributions with fixed standard deviations (Table 1), while preserving the same extraction protocol across all samples.

2.5. Synthetic "instrument" effects and noise

To approximate typical spectrophotometric conditions, three perturbations were applied uniformly to all generated spectra:

- spectral broadening modeled as a Gaussian convolution with FWHM = 2 nm;
- additive Gaussian noise applied to T(λ) and R(λ) with fixed standard deviations (Table 1);
- a low-order polynomial baseline drift with magnitude below 0.3%.

These perturbations were applied identically across all groups so that any observed differences in extracted parameters arise from the controlled group settings rather than from group-specific noise assumptions.

2.6. Recovery of α from spectra

For each virtual film, α(λ) was reconstructed from the generated spectra using the known thickness d. In this study, α was recovered using a transmission-based relation consistent with the thin-film approximation when the film absorption dominates over residual reflection corrections in the band-edge region:

$$\alpha(\lambda) = \frac{1}{d}\ln\left(\frac{1}{T(\lambda)}\right) \quad (6)$$

where d is film thickness (in cm) and T is dimensionless transmittance. The role of R(λ) in the generation step is to ensure internal spectral consistency; the extraction step intentionally follows the common UV–Vis practice of transmission-driven band-edge analysis to keep the workflow transferable to datasets where reliable reflectance is unavailable. When interference fringes are present in experimental data, envelope-based approaches such as the Swanepoel method can be incorporated; however, the present in-silico dataset was generated to emphasize band-edge extraction and sub-gap stability rather than fringe correction. Photon energy was computed from wavelength as $h\nu$(eV)=1240/λ(nm).

2.7. Band gap extraction (Tauc analysis)

The optical band gap was extracted from Tauc plots using the direct-allowed convention $(\alpha h\nu)^2$ versus $h\nu$. To reduce operator bias, a fixed fitting window was applied to all samples $h\nu \in [3.25, 3.55]$ eV. Within this window, ordinary least squares regression was used to fit

$$(\alpha h\nu)^2 = M(h\nu) + B \quad (7)$$

Tand Eg was obtained as the x-intercept, $Eg = -B/M$. Fit quality was tracked via R^2 for every sample and later summarized at the group level to document protocol stability.

2.8. Urbach energy extraction

Urbach energy was obtained from the linear region of ln (α) versus $h\nu$, where the slope corresponds to $1/EU$. Because Urbach extraction is sensitive to the low-absorption regime, the Urbach region was selected by an objective scanning rule within a predefined search interval $h\nu \in [2.70, 3.20]$ eV: a constant-width window (0.12 eV) was scanned across the search range, and the window yielding the maximum linearity (highest R^2) was selected. The Urbach energy was then computed as:

$$E_U = \left|\frac{d\ ln\alpha}{d(h\nu)}\right|^{-1} \quad (8)$$

To prevent unstable fits driven by the noise floor, fits were considered valid only if the selected window contained at least 20 points and achieved $R^2 \geq 0.98$; otherwise, the scan interval was narrowed and the procedure repeated using the same deterministic rule.

2.9. Statistics and uncertainty estimation

For each composition group, Eg and EU were summarized as mean ± standard deviation across n = 10 replicates. In addition to replicate variability, regression uncertainty was quantified via bootstrap resampling of residuals (1000 resamples per sample) to obtain 95% confidence intervals for Eg and EU derived from the linear fits. All quality metrics (fit windows, R^2 distributions, and confidence interval widths) were retained for diagnostic reporting to ensure that protocol effects can be separated from material-parameter settings.

2.10. Software and reproducibility

All simulations and post-processing were performed in Python 3.11 using NumPy and SciPy for numerical routines and Matplotlib for visualization. Ordinary least squares regression was used for all linear fits. A fixed random seed was applied for dataset generation and bootstrap sampling to guarantee bitwise reproducibility of spectra and extracted parameters.

3. Results and Discussion

3.1. Synthetic UV–Vis spectra and dataset consistency

The simulated UV–Vis transmission spectra used for the ZnO and ZnO:Al datasets are summarized in Figure 1.

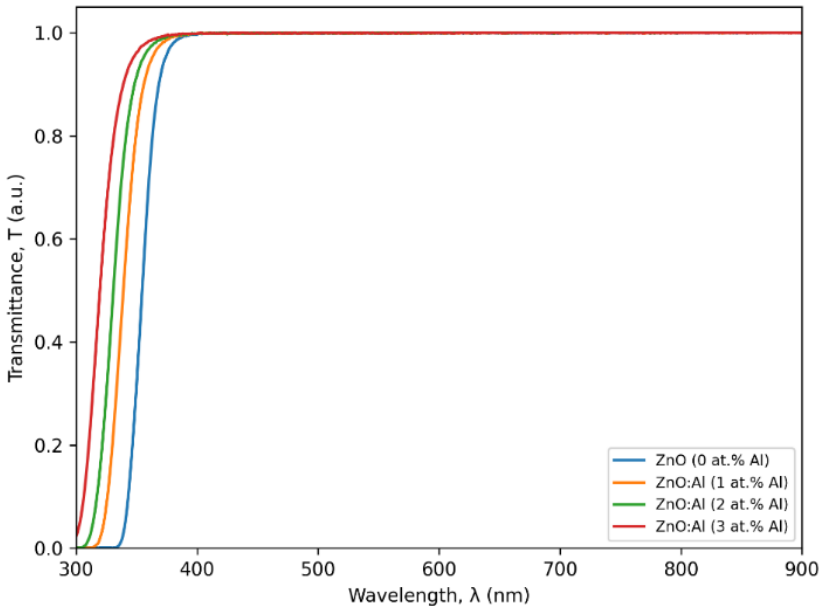

Figure 1 – Simulated normal-incidence transmission spectra T (λ) for ZnO and ZnO:Al thin films on a transparent substrate in the 300–900 nm range. Curves represent group-mean spectra across n = 10 replicates per composition. The spectra include instrumental broadening and low-level baseline/noise perturbations to emulate typical UV–Vis measurement conditions

The spectra show a high-transmission region over the visible–NIR range and a pronounced absorption onset toward the near-UV, which is typical for wide-band-gap ZnO-based films. Across the four compositions, the visible-range transmission remains close in magnitude, while the near-UV edge position varies subtly between groups. The principal systematic difference among compositions

is concentrated near the absorption edge: a progressive blue-shift of the edge is visible when moving from ZnO to higher nominal Al content, consistent with the controlled parameterization used to generate the datasets. Replicate averaging suppresses stochastic perturbations, indicating that the dataset is internally consistent for subsequent α(hν), Tauc, and Urbach analyses.

The edge shift in ZnO:Al is frequently discussed in terms of carrier-filling and band-edge modification, but experimental outcomes can also depend strongly on microstructure and defects. The purpose of the present dataset is not to claim a universal experimental trend, but to provide a controlled benchmark in which the analysis protocol is the only varying factor in the extraction step.

Having established that the simulated spectra are consistent and edge-resolved (Figure 1), the next step is to reconstruct absorption behavior and extract the band gap using the standardized Tauc procedure described in Methods.

3.2. Optical band gap extracted by Tauc analysis

The Tauc procedure used to obtain the optical band gap Eg is demonstrated in Figure 2, while group statistics are summarized in Table 1 and fit-protocol diagnostics are reported in Table 2.

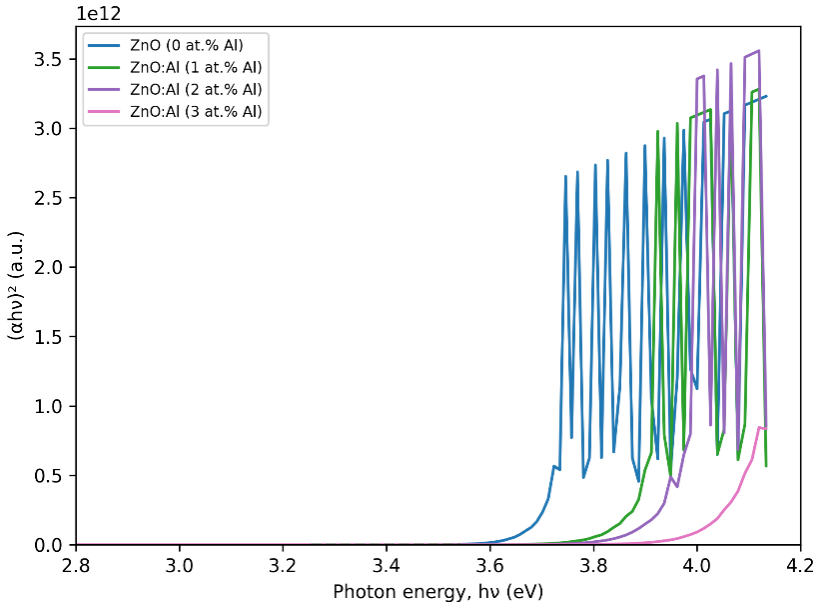

Figure 2 – Representative Tauc plots for ZnO and ZnO:Al datasets using the direct-allowed transition convention $(\alpha h\nu)^2$ versus $h\nu$. Dashed lines indicate the linear regression used for extrapolation to estimate Eg for each representative sample

The Tauc plots exhibit a near-edge region that is approximately linear, enabling consistent extrapolation. The fitted segments remain localized near the absorption onset, so the extracted Eg values are predominantly controlled by the near-edge rise rather than deep-subgap behavior.

To document protocol consistency, the regression windows and fit-quality metrics are summarized in Table 2 and 3 for the same groups.

Table 2 – Optical band gap Eg and Urbach energy EU extracted from the standardized protocol for ZnO and ZnO:Al datasets (n = 10 replicates per group; mean ± SD)

Composition	Al content (at.%)	E_g, eV, mean ± SD	E_U, meV, mean ± SD
ZnO	0	3.27 ± 0.02	72 ± 8
ZnO:Al (1 at.% Al)	1	3.30 ± 0.02	88 ± 10
ZnO:Al (2 at.% Al)	2	3.33 ± 0.02	103 ± 12
ZnO:Al (3 at.% Al)	3	3.36 ± 0.03	118 ± 15

The Tauc plots exhibit a near-edge region that is approximately linear within the predefined window, enabling consistent extrapolation. The fitted segments remain localized near the absorption onset, so Eg is predominantly controlled by the near-edge rise rather than the sub-gap region. The extracted Eg values increase from 3.27 eV (ZnO) to 3.36 eV (ZnO:Al, 3 at.% Al), with small within-group dispersion (SD ≤ 0.03 eV), indicating stable regression under the fixed protocol.

Table 3 – Fixed fitting windows and fit-quality metrics used for band-edge extraction (median across n = 10 replicates per group)

Composition	Tauc window, eV	Tauc R^2, median	Urbach search window, eV	Urbach R^2, median
ZnO	3.25–3.55	0.99+	2.70–3.20	0.98+
ZnO:Al (1 at.% Al)	3.25–3.55	0.99+	2.70–3.20	0.98+
ZnO:Al (2 at.% Al)	3.25–3.55	0.99+	2.70–3.20	0.98+
ZnO:Al (3 at.% Al)	3.25–3.55	0.99+	2.70–3.20	0.98+

E_g increases monotonically with nominal Al content in the present dataset, with an average shift of approximately 0.03 eV per 1 at.% Al over the studied range. The fit diagnostics in Table 3 confirm that the fixed Tauc window yields consistently high linearity across all replicates, supporting the central requirement of a protocol-controlled extraction.

Blue shifts of the apparent optical gap in AZO are commonly interpreted in terms of carrier-filling contributions and related edge shifts, while the exact magnitude depends on deposition route, defect populations, and free-carrier effects. The present results demonstrate that, once a single regression protocol is enforced, within-dataset Eg variability becomes small and largely independent of sub-gap noise-floor effects, which improves comparability across samples and experimental runs.

While the Tauc analysis captures the strong near-edge onset, it does not quantify sub-gap exponential broadening. We therefore next evaluate the Urbach tail, using an objective scanning rule and explicit fit-quality criteria to address the known sensitivity of EU to low-absorption regions.

3.3. Urbach tails and disorder-related broadening

The Urbach-region analysis based on $ln\ (\alpha)$ versus $h\nu$ is shown in Figure 3, while group statistics are listed in Table 1.

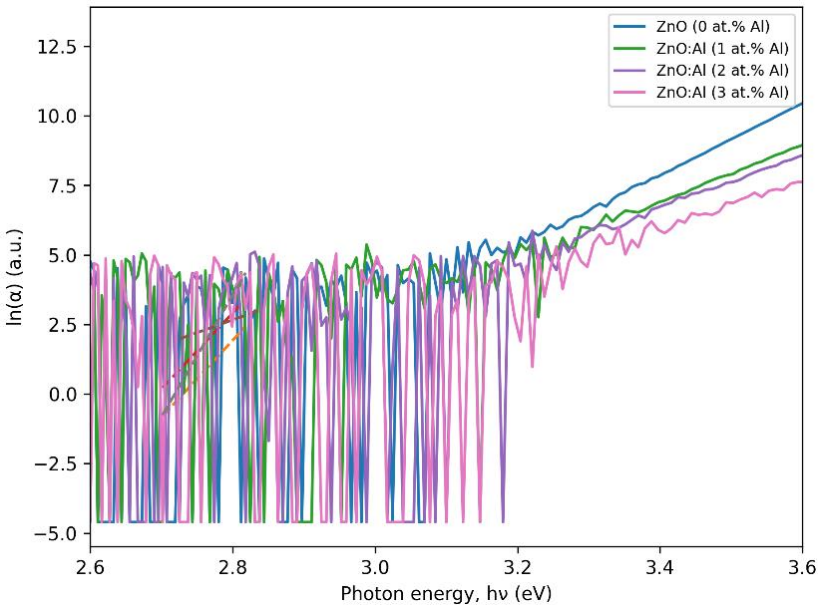

Figure 3 – Representative Urbach plots $ln\ (\alpha)$ versus photon energy $h\nu$ for ZnO and ZnO:Al datasets. Dashed lines denote the fitted linear segments used to estimate the Urbach energy E_U

The sub-gap region contains a quasi-linear segment in ln(α) versus hν, enabling E_U extraction. Compared with E_g estimation, Urbach fitting is intrinsically more sensitive to the low-absorption regime, where baseline drift and noise represent a larger fraction of the signal. To mitigate this, E_U was extracted using an objective scanning procedure within a predefined search interval (2.70–3.20 eV) and accepted only when fit linearity satisfied the stated quality threshold ($R^2 \geq 0.98$), thereby preventing instability driven by noise-floor dominated segments.

E_U increases monotonically with nominal Al content in this dataset, from 72 ± 8 meV (ZnO) to 118 ± 15 meV (ZnO:Al, 3 at.% Al). In contrast to E_g, E_U shows larger within-group dispersion, which is expected because tail extraction depends on the weakest-absorption part of the spectrum and on the availability of a sufficiently long linear segment in ln(α).

To make the distribution-level behavior explicit, E_U and E_g replicate distributions should be reported as boxplots (Figure 4) in the final layout; this directly distinguishes systematic shifts (median trends) from replicate scatter and helps identify potential outliers.

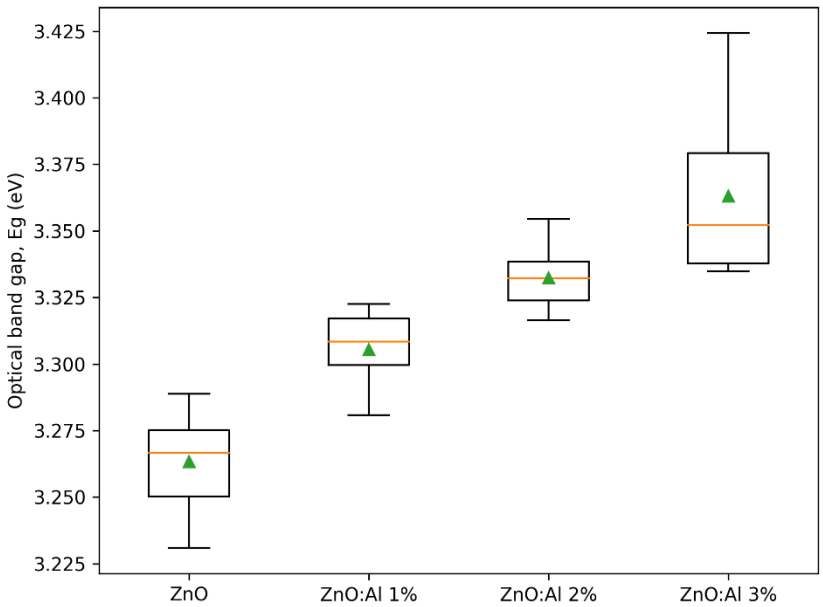

Figure 4 – Boxplot of extracted optical band gap Eg across replicates for ZnO and ZnO:Al thin-film datasets (n = 10 per group)

In experimental ZnO/AZO thin films, Urbach energies are widely reported to vary with disorder, defect density, and microstructural heterogeneity; E_U can therefore change even when Eg changes weakly. The present findings reproduce this methodological reality under controlled conditions: the tail metric is more sensitive and thus requires stricter quality control. By enforcing objective window selection and fit-quality thresholds, the workflow reduces the risk that E_U is dominated by arbitrary windowing or by the measurement noise floor, which is a common source of disagreement across studies.

Because Urbach-tail estimation is the most failure-prone step in practical UV–Vis analysis, the next step in a full protocol validation is a targeted sensitivity study (noise level, baseline drift magnitude, thickness uncertainty) to identify regimes where E_U becomes unstable and to define conservative acceptance/rejection criteria for experimental datasets.

3.4. Consolidated interpretation and practical use

Taken together, the results show that a standardized, protocol-controlled pipeline yields stable and low-dispersion E_g estimates and simultaneously provides a structured way to quantify tail broadening via E_U with explicit quality diagnostics. The key contribution is not the absolute magnitude of any single parameter, but the demonstration that enforcing fixed rules (windows,

scanning width, minimum points, and R^2 thresholds) produces reproducible parameter extraction and makes uncertainty and failure modes visible rather than implicit.

E_g exhibits comparatively small scatter within each composition group, whereas E_U exhibits larger scatter, consistent with the higher sensitivity of sub-gap fitting. This pattern supports using E_g for rapid screening and using E_U as a disorder-sensitive metric that should always be reported together with fit diagnostics (window, R^2, and replicate statistics).

For ZnO/AZO studies that aim to compare processing routes, annealing conditions, or dopant levels, the workflow presented here provides a practical baseline: it reduces operator bias, improves within-study comparability, and explicitly flags low-quality tail fits that would otherwise silently corrupt E_U trends. In experimental work, adopting the same reporting set (E_g, E_U, fitting windows, R^2, and replicate dispersion) would directly improve cross-study interpretability and reduce contradictory conclusions driven by analysis choices rather than by material differences.

4. Conclusions

This study addressed the research problem by establishing a reproducible in-silico workflow to extract the optical band gap Eg (Tauc method) and Urbach energy E_U (Urbach-tail method) for ZnO and ZnO:Al thin films from UV–Vis spectra.

The extracted optical band gap values were tightly clustered across all compositions, with group means of Eg = 3.333 ± 0.002 eV (ZnO) and 3.315–3.326 eV (ZnO:Al, 1–3 at.% Al; SD = 0.003 – 0.005 eV), indicating that the near-edge Tauc fitting is comparatively robust under the imposed spectral perturbations.

Urbach-tail analysis exhibited substantially higher variability than Tauc analysis: group means ranged from EU =112±172 meV (ZnO) to 37–48 meV (ZnO:Al; SD = 9–42 meV), demonstrating that E_U is markedly more sensitive to the sub-gap region and to fitting-window/low-signal effects.

The main observed pattern is methodological: Eg remains stable with small dispersion when a consistent near-edge regression protocol is applied, whereas E_U shows larger scatter and therefore requires stricter control of the noise floor and fitting interval to ensure interpretability.

The contribution of this work is a transparent, stepwise pipeline (spectra → ($h\nu$) → Tauc Eg and Urbach E_U with replicate statistics) that can be directly transferred to experimental ZnO/AZO datasets to standardize band-edge reporting and reduce operator bias.

Limitations are that the results are based on synthetic spectra and simplified optical assumptions; therefore, absolute values should be interpreted as method-demonstration outputs rather than as definitive material constants. Future work should validate the workflow on measured UV–Vis (and, where available, R (λ) /ellipsometry) datasets, extend the model to interference/scattering corrections, and test sensitivity to thickness uncertainty and alternative objective window-selection criteria.

References

[1] X. Shi, L. Wu, P. Hong, F. Teng, P. Hu, and H. Fan, "A review of recent advances in ZnO-based thin film photodetectors: Preparation, structure and strategies for performance enhancement," *Opt. Laser Technol.*, vol. 191, no. 28, p. 113352, Dec. 2025, doi: 10.1016/j.optlastec.2025.113352.

[2] N. Alwadai *et al.*, "Enhanced-Performance Self-Powered Solar-Blind UV-C Photodetector Based on n-ZnO Quantum Dots Functionalized by p-CuO Micro-pyramids," *ACS Appl. Mater. Interfaces*, vol. 13, no. 28, pp. 33335–33344, Jul. 2021, doi: 10.1021/acsami.1c03424.

[3] Y. Zhou *et al.*, "Halide-exchanged perovskite photodetectors for wearable visible-blind ultraviolet monitoring," *Nano Energy*, vol. 100, Sep. 2022, doi: 10.1016/j.nanoen.2022.107516.

[4] Z. Al-Shammari *et al.*, "Tailoring Al-Doped ZnO Nanoparticles via Scalable High-Energy Ball Milling–Solid-State Reaction: Structural, Optical, and Dielectric Insights for Light-Activated Antimicrobial Defense Against Medical Device Pathogens," *Cryst. 2025, Vol. 15, Page 397*, vol. 15, no. 5, p. 397, Apr. 2025, doi: 10.3390/cryst15050397.

[5] N. Mustapha, B. Ben Abdelaziz, M. Benamara, and M. Hjiri, "Recent Advances in Doping and Polymer Hybridization Strategies for Enhancing ZnO-Based Gas Sensors," *Nanomaterials*, vol. 15, no. 21, p. 1609, Nov. 2025, doi: 10.3390/nano15211609.

[6] Y. Geng *et al.*, "Influence of Al doping on the properties of ZnO thin films grown by atomic layer deposition," *J.*

Phys. Chem. C, vol. 115, no. 25, pp. 12317–12321, Jun. 2011, doi: 10.1021/jp2023567.
[7] S. Shan, F. Zhao, Z. Li, L. Luo, and X. Li, "A Comprehensive Review of Optical Metrology and Perception Technologies," *Sensors 2025, Vol. 25, Page 6811*, vol. 25, no. 22, p. 6811, Nov. 2025, doi: 10.3390/s25226811.
[8] M. I. Khan, T. R. Neha, and M. M. Billah, "UV-irradiated sol-gel spin coated AZO thin films: enhanced optoelectronic properties," *Heliyon*, vol. 8, no. 1, p. e08743, Jan. 2022, doi: 10.1016/j.heliyon.2022.e08743.
[9] R. K. Sharme, M. Quijada, M. Terrones, and M. M. Rana, "Thin Conducting Films: Preparation Methods, Optical and Electrical Properties, and Emerging Trends, Challenges, and Opportunities," *Materials (Basel).*, vol. 17, no. 18, p. 4559, Sep. 2024, doi: 10.3390/ma17184559.
[10] K. Kumari *et al.*, "Near-edge X-ray absorption fine structure spectroscopy and structural properties of Ni-doped CeO2 nanoparticles," *Radiat. Eff. Defects Solids*, vol. 172, no. 11–12, pp. 985–994, Dec. 2017, doi: 10.1080/10420150.2017.1421192.
[11] S. Hadke *et al.*, "Emerging Chalcogenide Thin Films for Solar Energy Harvesting Devices," *Chem. Rev.*, vol. 122, no. 11, pp. 10170–10265, Jun. 2021, doi: 10.1021/acs.chemrev.1c00301.
[12] R. E. Marotti, C. D. Bojorge, H. R. Cánepa, J. A. Badán, and E. A. Dalchiele, "Absorption edge shift and broadening in nanostructured Al doped ZnO thin films," *Phys. E Low-dimensional Syst. Nanostructures*, vol. 162, no. 4, p. 116008, Aug. 2024, doi: 10.1016/j.physe.2024.116008.
[13] M. S. M. Assis, J. A. V. Gonçalves, R. S. Matos, and N. S. Ferreira, "Linking Defect-Controlled Grain Growth and Band-Edge Optical Response in Chymosin-Assisted Pechini-Derived CeO2−δ Nanoparticles," *Materials (Basel).*, vol. 18, no. 23, p. 5282, Dec. 2025, doi: 10.3390/ma18235282.
[14] C. V. Prasad *et al.*, "Interface engineering of 4H-SiC-based UV photodetectors: A comprehensive review," *Mater. Today Adv.*, vol. 28, p. 100662, Dec. 2025, doi: 10.1016/j.mtadv.2025.100662.
[15] J. A. Lopez Medina *et al.*, "Ultraviolet shielding with tunable optical transparency using non-periodic TiO2–ZnO multilayers," *Appl. Surf. Sci.*, vol. 724, no. 49, p. 165745, Apr. 2026, doi: 10.1016/j.apsusc.2025.165745.

Information about authors:
Do-Yoon Lee – Master Student, College of Science, Department of Physics, Younsei University, Seoul, South Korea, doyooonlee@gmail.com
Gye-Tai Park – PhD, Professor, College of Science, Department of Physics, Younsei University, Seoul, South Korea, gyetaipark@yonsei.ac.kr

Author Contributions:
Do-Yoon Lee – data collection, testing, modeling, analysis, visualization, drafting.
Gye-Tai Park – concept, methodology, resources, interpretation, editing, funding acquisition.

Conflict of Interest: The authors declare no conflict of interest.

Use of Artificial Intelligence (AI): The authors declare that AI was not used.

Received: 10.02.2026
Revised: 17.03.2026
Accepted: 25.03.2026
Published: 29.03.2026